nature nanotechnology

LETTERS

https://doi.org/10.1038/s41565-019-0521-z

Remotely controlled chemomagnetic modulation of targeted neural circuits

Siyuan Rao[1,2], Ritchie Chen[2,3], Ava A. LaRocca[4], Michael G. Christiansen[1,4,5], Alexander W. Senko[1,4], Cindy H. Shi[4], Po-Han Chiang[1], Georgios Varnavides[1,4,6], Jian Xue[7,8], Yang Zhou[7,8], Seongjun Park[1,9], Ruihua Ding[6,10], Junsang Moon[1,4], Guoping Feng[7,8] and Polina Anikeeva[1,4,7,8]*

Connecting neural circuit output to behaviour can be facilitated by the precise chemical manipulation of specific cell populations[1,2]. Engineered receptors exclusively activated by designer small molecules enable manipulation of specific neural pathways[3,4]. However, their application to studies of behaviour has thus far been hampered by a trade-off between the low temporal resolution of systemic injection versus the invasiveness of implanted cannulae or infusion pumps[2]. Here, we developed a remotely controlled chemomagnetic modulation—a nanomaterials-based technique that permits the pharmacological interrogation of targeted neural populations in freely moving subjects. The heat dissipated by magnetic nanoparticles (MNPs) in the presence of alternating magnetic fields (AMFs) triggers small-molecule release from thermally sensitive lipid vesicles with a 20 s latency. Coupled with the chemogenetic activation of engineered receptors, this technique permits the control of specific neurons with temporal and spatial precision. The delivery of chemomagnetic particles to the ventral tegmental area (VTA) allows the remote modulation of motivated behaviour in mice. Furthermore, this chemomagnetic approach activates endogenous circuits by enabling the regulated release of receptor ligands. Applied to an endogenous dopamine receptor D1 (DRD1) agonist in the nucleus accumbens (NAc), a brain area involved in mediating social interactions, chemomagnetic modulation increases sociability in mice. By offering a temporally precise control of specified ligand–receptor interactions in neurons, this approach may facilitate molecular neuroscience studies in behaving organisms.

The local delivery of neuromodulators within the brain allows the linking of their molecular targets to behaviour[5]. A systemic delivery of compounds via intravenous or intraperitoneal injection does not permit localized chemical neuromodulation and may be accompanied by off-target effects, with efficacy further impeded by the limited blood–brain barrier permeability[6]. Consequently, permanently implanted cannulae are typically used for the local delivery of compounds to the neural circuits of interest[7]. To facilitate the spatially restricted and remotely controlled delivery of neuromodulators to neural targets, we sought to gate the release of small molecules using non-invasive stimuli. We applied weak AMFs with frequencies of hundreds of kilohertz, that can access arbitrarily deep tissue volumes[8,9] to produce hysteretic heating by MNPs. MNP heating in AMFs is extensively applied in cancer hyperthermia[10], and was recently leveraged to control cellular signalling[8,11], gene expression[12] and mouse behaviour by triggering heat-sensitive ion channels[13]. Here, we applied AMF stimulation to remotely control the release of chemical compounds from thermally sensitive liposomes loaded with MNPs. Multiple microdoses could be delivered through liposome permeabilization on the localized AMF-triggered heating of MNPs, whereas negligible leakage was observed in the absence of an AMF. When combined with the chemogenetic neuromodulation approach, designer receptors exclusively activated by designer drugs (DREADDs)[4,14], this method decreased the response time from hours to tens of seconds at multiple time points within genetically defined neural populations. This scheme was further generalized to endogenous circuits by enabling the local delivery of receptor agonists and antagonists, and thus facilitate the dissection of behaviour by activating ligand–receptor pairs.

We designed a chemomagnetic gate that consisted of thermally responsive (MNP-loaded) liposomes composed of a mixture of the 1,2-dipalmitoyl-sn-glycero-3-phosphocholine (DPPC) and 1,2-distearoyl-sn-glycero-3-phosphocholine (DSPC) lipids and cholesterol (10:5:3 weight ratio)[15,16] with a phase-transition temperature of 43 °C (Fig. 1a). To synthesize magnetic liposomes loaded with chemical neuromodulators, we used a double-emulsion method[15] (Supplementary Fig. 1). In brief, MNPs and the payload were solubilized in an aqueous phase, and then transferred into a solution of amphiphilic lipids in a hydrophobic solvent. After homogenization, the aqueous phase that contained MNPs and the payload was encapsulated within the lipid micelles, and a rapid evaporation of the hydrophobic phase produced double-micelle magnetoliposomes with diameters of 426 ± 346 nm (Fig. 1b). The magnetoliposomes maintained their structural integrity after 40 s of exposure to an AMF ($H_0 = 45 \pm 2$ mT, $f = 150$ kHz), which indicates their stability across multiple release cycles (Fig. 1b). As the latency of release after the AMF application scales inversely with the MNP heating efficiency (specific loss power), for physiologically safe AMFs with a frequency $f = 150$ kHz and amplitudes $H_0 \leq 60$ mT (ref. [17]), 25 nm iron oxide MNPs were selected[18]. Their specific loss power values were calorimetrically measured (741 ± 30 W $g_{[Fe]}^{-1}$, $H_0 = 45 \pm 2$ mT,

[1]Research Laboratory of Electronics, Massachusetts Institute of Technology, Cambridge, MA, USA. [2]Simons Center for Social Brain, Massachusetts Institute of Technology, Cambridge, MA, USA. [3]Department of Bioengineering, Stanford University, Stanford, CA, USA. [4]Department of Materials Science and Engineering, Massachusetts Institute of Technology, Cambridge, MA, USA. [5]Department of Health Sciences and Technology at the Swiss Federal Institute of Technology in Zürich (ETHZ), Zürich, Switzerland. [6]John A. Paulson School of Engineering and Applied Sciences, Harvard University, Cambridge, MA, USA. [7]McGovern Institute for Brain Research, Massachusetts Institute of Technology, Cambridge, MA, USA. [8]Department of Brain and Cognitive Sciences, Massachusetts Institute of Technology, Cambridge, MA, USA. [9]Department of Electrical Engineering and Computer Science, Massachusetts Institute of Technology, Cambridge, MA, USA. [10]Department of Chemistry and Chemical Biology, Harvard University, Cambridge, MA, USA. *e-mail: anikeeva@mit.edu

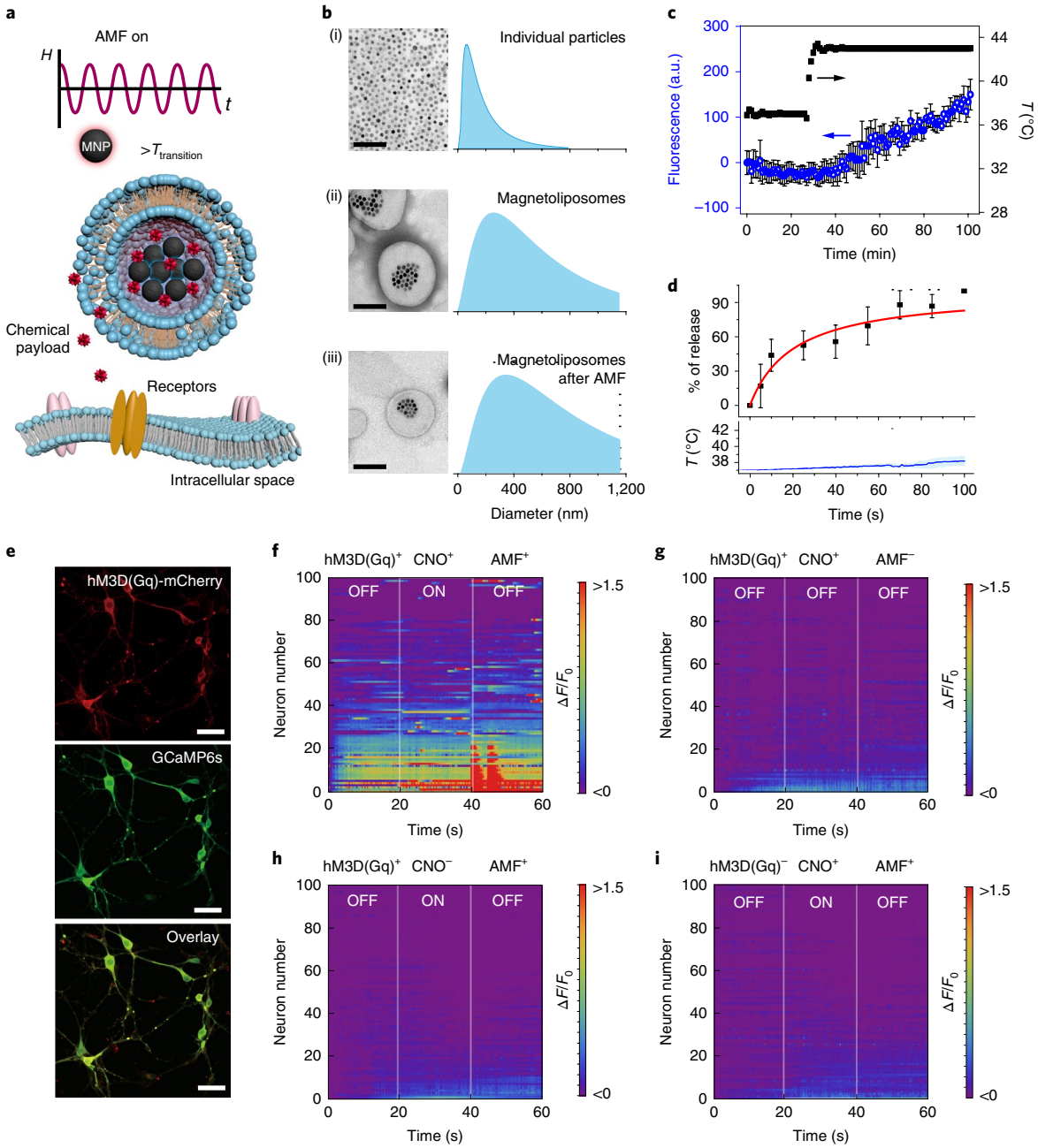

Fig. 1 | Magnetically controlled chemical payload release. a, Experimental scheme of the AMF-triggered chemical payload release from the magnetoliposomes. **b**, Transmission electron microscope images and the size distributions from dynamic light scattering spectra of the MNPs before (i) and after (ii) encapsulation into the magnetoliposomes, and the magnetoliposomes after exposure to 40 s of an AMF ($H_0 = 45 \pm 2$ mT and $f = 150$ kHz) (iii). Scale bars, 200 nm. **c**, Fluorescent dye (Alexa Fluor 488) release from the magnetoliposomes (mean ± s.d., $n = 3$ independent samples) during the bath temperature increase from 37 to 43 °C. **d**, AMF-triggered dye release (mean ± s.d., $n = 3$ independent samples) from magnetoliposomes and the temperature profile of the bulk solution (solid line: mean, shaded area: s.d. n = 3). **e**, Confocal images of the primary hippocampal neurons that express hSyn::hM3D(Gq)-mCherry and hSyn::GCaMP6s. Scale bar, 50 µm. The experiment was repeated three times independently with similar results. **f**–**i**, Heat maps of the normalized GCaMP6s fluorescence intensity of 100 automatically selected neurons in different experimental conditions. F_0 is defined as the mean of the fluorescence intensity during the first 10 s. ON, AMF is turned on; OFF, AMF is turned off. AMF conditions: $H_0 = 45 \pm 2$ mT, $f = 150$ kHz, 20 s. hM3D(Gq)$^+$, neurons are expressing hSyn::hM3D(Gq)-mCherry. hM3D(Gq)$^-$, neurons are expressing hSyn::mCherry. CNO$^+$, CNO is encapsulated in magnetoliposomes. CNO$^-$, CNO is not encapsulated in magnetoliposomes. AMF$^+$, AMF stimulus is applied. AMF$^-$, AMF stimulus is not applied. a.u., arbitrary units.

$f = 150$ kHz) using a custom AMF coil driven by a resonant circuit (Supplementary Fig. 2)[19]. Using fluorescent dye as a payload, a minimal background leakage from the liposomes was observed at 37 °C. Gradual release was observed when the temperature exceeded the lipid phase-transition point of 43 °C (Fig. 1c). Release of the payload due to the local MNP heating within the magnetoliposomes scaled with the duration of the AMF stimulus, whereas only a negligible increase in the bulk solution temperature was observed (Fig. 1d).

Chemomagnetic modulation of the cell function was first evaluated in vitro. Owing to their minimal cross-reactivity with endogenous receptors, DREADDs have become indispensable tools for chemogenetic neuromodulation[3,14]. We therefore selected DREADDs as the targets for the chemomagnetic control of intracellular calcium (Ca^{2+}) in rat primary hippocampal neurons (Fig. 1e–i) and human embryonic kidney (HEK293FT) cells (Supplementary Fig. 3). Hippocampal cells were either transduced with an adeno-associated virus serotype 9 (AAV9) that carried a depolarizing DREADD hM3D(Gq), commonly used for chemogenetic neural excitation[3], fused to a red fluorescent protein mCherry (AAV9-hSyn::hM3D(Gq)-mCherry ($hM3D(Gq)^+$)) or with an AAV9 that carried a fluorophore alone (AAV9-hSyn::mCherry ($hM3D(Gq)^-$)). The cells were also transduced with an AAV9 that carried a fluorescent calcium indicator, GCaMP6s (hSyn::GCaMP6s), to record the intracellular Ca^{2+} changes as a proxy for membrane depolarization (Fig. 1e)[20]. The GCaMP6s and hM3D(Gq) expression and function were first corroborated by fluorescence imaging of the Ca^{2+} influx in response to the hM3D(Gq) ligand clozapine N-oxide (CNO) (Supplementary Fig. 4). By applying an AMF in the presence of magnetoliposomes that encapsulated CNO, over 60% of the $hM3D(Gq)^+$ neurons exhibited synchronized firing after the stimulus (Fig. 1f and Supplementary Fig. 5), whereas only sporadic activity was observed in $hM3D(Gq)^-$ neurons (or in the absence of stimuli) (Fig. 1g–i). This implies that the CNO release from the magnetoliposomes in the presence of the AMF was necessary and sufficient to trigger hM3D(Gq) and cause membrane depolarization in the neurons while avoiding non-specific thermal effects. The latter was corroborated by the chemomagnetic stimulation of HEK293FT cells that expressed the heat-sensitive transient receptor potential cation channel subfamily V member 1 (TRPV1) (CamKIIα::TRPV1-p2A-mCherry) that did not show a significant response to an AMF in the presence of magnetoliposomes (Supplementary Fig. 6). An analogous experimental scheme was also implemented with neurons that expressed inhibitory DREADD hM4D(Gi), and neural inhibition was observed following AMF stimulation in the presence of CNO-loaded magnetoliposomes, which indicates future opportunities in bi-directional control (Supplementary Fig. 7).

We next tested the chemomagnetic neural excitation approach in the mouse VTA, a deep brain structure. The VTA, and its projection circuits, have been extensively researched in the context of motivated and social behaviours[21], reward processing[22], substance abuse[23] and depression[24], which makes this region a robust and biologically important target of neuromodulation techniques[25]. A broad expression of hM3D(Gq)-mCherry in VTA neurons was observed after AAV delivery (AAV5-hSyn::hM3D(Gq)-mCherry or AAV5-hSyn::mCherry) (Fig. 2a). After an incubation period of 5–6 weeks, magnetoliposomes were injected into the same region (Fig. 2a), and the anaesthetized mice were transferred into a custom coil with a $\pi \times 3.5 \times 3.5 \times 5\,cm^3$ working volume[19] and subjected to a sequence of five AMF cycles ($f = 164\,kHz$ and $H_0 = 45 \pm 2\,mT$) with 40 s ON epochs, followed by 40 s OFF rest periods (Supplementary Fig. 8). To predict the payload distribution after the AMF stimulation, we used an Abaqus drug diffusion model that quantified the CNO concentration. We found that a 1 µl injection of CNO-loaded magnetoliposomes was sufficient to activate hM3D(Gq) across the entire VTA after 40 s of AMF stimulus and a 5 min diffusion period (Supplementary Fig. 9). Bulk heating was not observed during the AMF stimulation for an identical volume and the concentration of magnetoliposome solution injected into a brain phantom (0.6% agarose gel) (Supplementary Fig. 10).

Immunofluorescence analysis of the expression of c-fos, an immediate early gene and a marker of neural activity[26], revealed that neuronal excitation in the VTA was only triggered by the AMF in mice expressing hM3D(Gq) and injected with CNO-loaded magnetoliposomes (Fig. 2b). Consistent with other neuromodulation techniques[8,21], neural activity in the VTA resulted in an upregulated c-fos expression in the downstream excitatory projection targets, the NAc and the medial prefrontal cortex (mPFC) (Fig. 2c,d). CNO-loaded magnetoliposomes remained effective for upregulating c-fos expression up to seven days after injection (Supplementary Figs. 11 and 12).

Neuronal excitation in response to the AMF-triggered release of CNO in the VTA was also photometrically recorded as a Ca^{2+}-dependent increase in the GCaMP6s fluorescence in mice freely moving within the AMF coil (Fig. 2e). Neurons in the VTA were transduced with an AAV9 cocktail that contained hSyn::hM3D(Gq)-mCherry (or a control plasmid hSyn::mCherry) and hSyn::GCaMP6s (Fig. 2f). A 5–6 week incubation period was followed by a magnetoliposome injection and optical fibre implantation. Consistent with the in vitro evaluation and c-fos expression, AMF robustly evoked a Ca^{2+} influx, as measured by GCaMP6s fluorescence, in the VTA of mice expressing hM3D(Gq) and injected with magnetoliposomes that contained CNO. No significant Ca^{2+} influx was found in mice that expressed the Ca^{2+} indicator alone or injected with magnetoliposomes that lacked the CNO payload (Fig. 2g).

Given the cellular effects observed in the VTA, we next tested whether chemomagnetic stimulation could shape behaviour in freely moving mice. As neural activity in the VTA is correlated with motivated behaviours[24], we hypothesized that mouse mobility in a forced swim test (FST) would be affected by the chemomagnetic stimulation. Akin to the c-fos quantification experiments described above, VTA neurons were transfected to express hM3D(Gq)-mCherry or mCherry alone under the hSyn promoter, and the magnetoliposomes were delivered after an incubation period of 5–6 weeks. After three days of recovery from the injection surgery, the mice were subjected to a FST assay for 6 minutes (Fig. 3) in a container placed within the AMF coil (Fig. 3a and Supplementary Fig. 13). The water level was set to position the VTA in the central area of the coil to ensure a uniform AMF amplitude during the entire stimulation epoch (Fig. 3b). It has been shown that repeated exposure of mice to the FST induces an adaptation manifested as a reduced baseline mobility[27]. To capture the dynamic range of the behavioural responses to the applied AMF, we developed a classifier for an unbiased automated selection of mice that exhibited such adaptation behaviour (Fig. 3c). The classifier fitted a linear combination of Gaussian distributions to the mobility data, and mice classified as belonging to a mobility distribution centred at around 0% prior to the AMF exposure were considered to have adapted (Fig. 3c). The mobility of the adapted mice was significantly enhanced by the CNO release in the VTA triggered during the 40 s AMF exposure, and the effect was conditional on hM3D(Gq) expression (Fig. 3d,e). In the absence of hM3D(Gq) expression, CNO loading in the magnetoliposomes or AMF exposure, the mobility did not vary significantly within the experimental trials. To determine the period of efficacy of the CNO release from the magnetoliposomes, we subjected the same cohort of adapted $hM3D(Gq)^+$ mice to the FST assay for three consecutive days. We repeatedly observed an increased mobility in response to the chemomagnetic stimulation (Fig. 3f), consistent with the stable on-demand release profiles found for the magnetoliposomes in cell cultures.

As the chemomagnetic approach is largely independent of the chemistry of water-soluble payloads, we sought to extend it to the modulation of non-modified, genetically intact neural circuits. Optogenetic excitation of the VTA projections to the NAc was previously shown to enhance social interactions in mice, and the effect could be blocked by the DRD1 antagonist SCH-23390[21]. Based on this evidence, we reasoned that the chemomagnetic release of a DRD1 agonist or antagonist in the NAc should influence social behaviour[28]. To test this hypothesis, the DRD1 agonist SKF-38393,

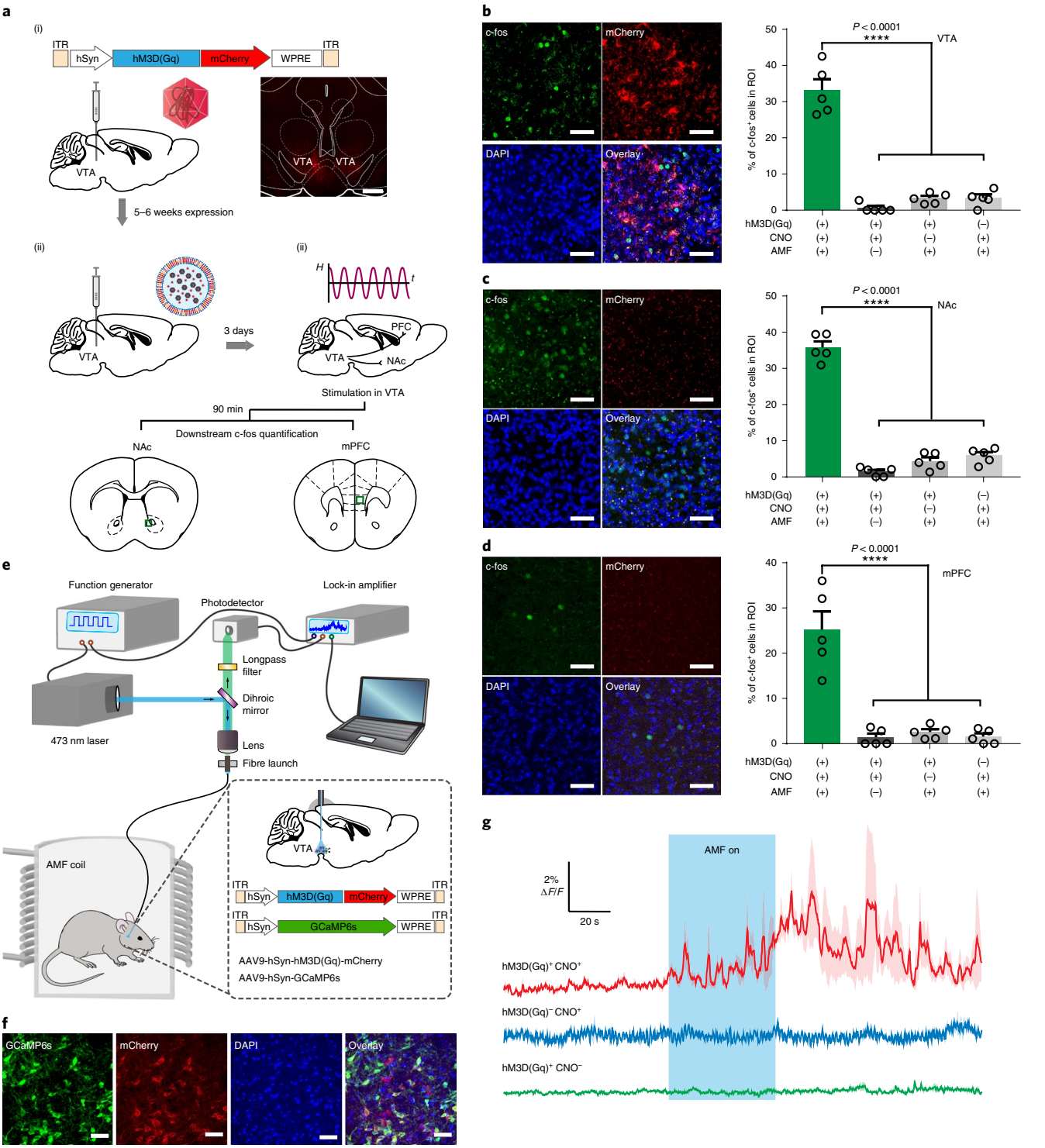

Fig. 2 | Chemomagnetic stimulation in vivo. a, Experimental timeline for the viral gene delivery (i), magnetoliposome injection (ii) and AMF stimulation (iii). Inset: a confocal image of the expression of hM3D(Gq)-mCherry in the mouse VTA. Scale bar, 200 µm. **b**–**d**, Left: confocal images of the c-fos expression in the VTA (**b**), NAc (**c**) and mPFC (**d**) of mice exposed to AMF (AMF$^+$), injected with CNO-loaded magnetoliposomes (CNO$^+$) and expressing hM3D(Gq) (hM3D(Gq)$^+$). Scale bars, 50 µm. Right: the percentages of c-fos that expresses (c-fos$^+$) neurons among 4,6-diamidino-2-phenylindole (DAPI)-labelled cells in each group (mean ± s.e.m.). An increased c-fos expression was observed after the chemomagnetic treatment as confirmed by one-way analysis of variance (ANOVA) and Tukey's multiple comparisons test ($n = 5$ mice, VTA $F_{3,16} = 86.29$, NAc $F_{3,16} = 207.6$, mPFC $F_{3,16} = 30.97$, $^{****}P < 0.0001$). All the c-fos quantification experiments were conducted in anaesthetized mice. **e**, Photometry set-up integrated with an AMF coil. **f**, Confocal images of the co-expression of GCaMP6s and hM3D(Gq)-mCherry in the mouse VTA. The experiment was repeated three times independently with similar results. Scale bars, 50 µm. **g**, Normalized dynamic fluorescence intensity change ($\Delta F/F_0$) of GCaMP6s in the VTA of mice freely moving within the AMF coil. A fluorescence increase was observed only on applying AMF stimulation in mice express hM3D(Gq) and injected with CNO-loaded magnetoliposomes (red). The blue area represents the AMF exposure. In all the experiments, $H_0 = 45 \pm 2$ mT, $f = 164$ kHz. Solid lines, mean; shaded areas, s.e.m., $n = 3$ mice for each test condition. ITR, inverted terminal repeat; ROI, region of interest; WPRE, woodchuck hepatitis virus posttranscriptional regulatory element.

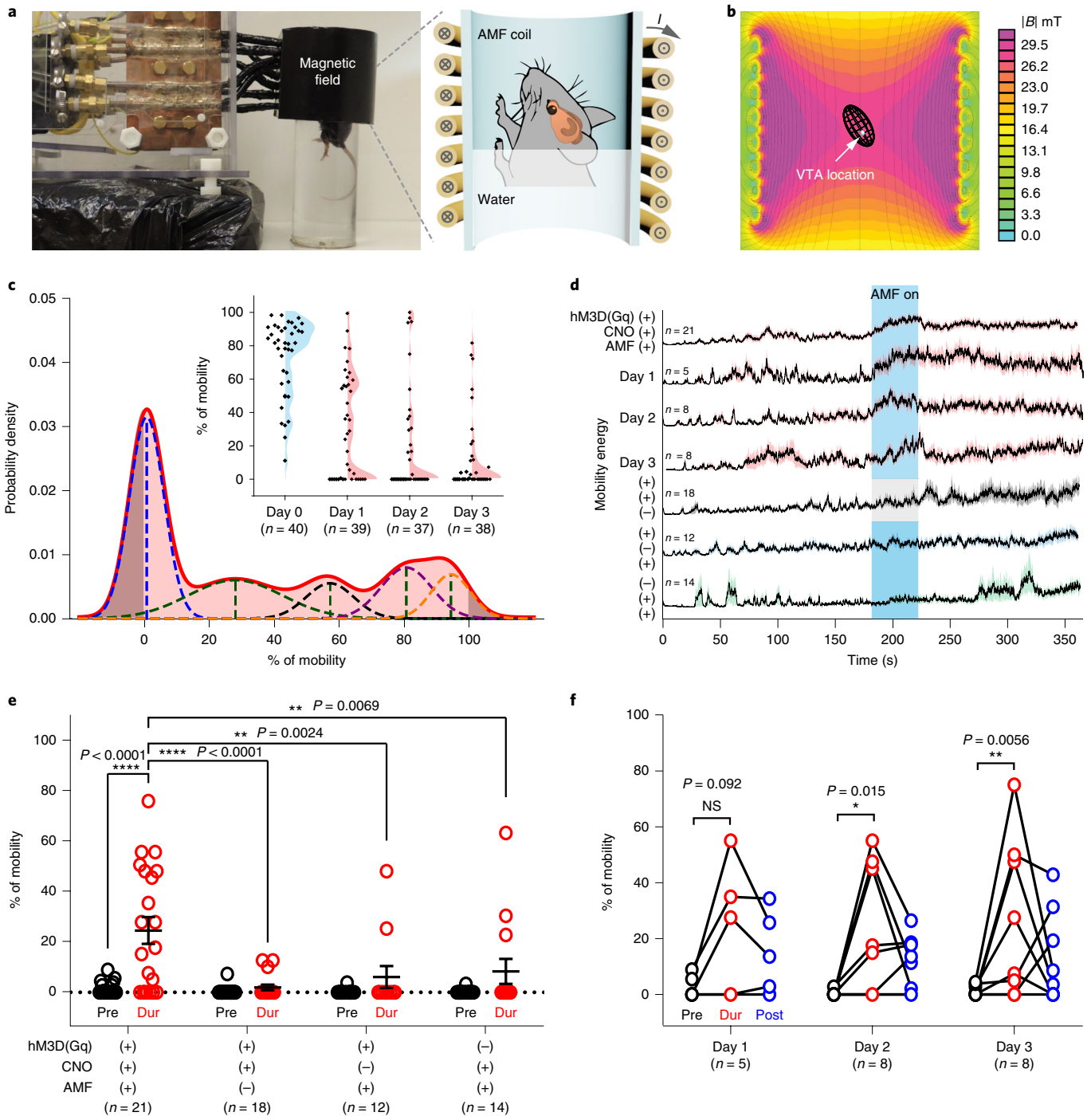

Fig. 3 | Remote chemomagnetic modulation of mouse behaviour using chemogenetics. a, A photograph and schematic of the FST assay within an AMF coil. **b**, The mouse VTA was situated within the region of the uniform AMF by adjusting the swimming tank water level. The colour map represents the cross-sectional view of the magnetic flux distribution as calculated by a finite element model for the AMF coil. **c**, Classification of the mouse baseline mobility to identify adaptation in the FST. Inset: the mobility percentage during the 6 min FST for all tested mice. The shaded areas display the Gaussian distribution of mouse mobility percentage on each day. Blue, training day (day 0); red, test days (days 1–3); *n*, number of test trials. **d**, Averaged motion energy curves for mice undergoing FST. The energy was calculated from the pixel changes in each frame of the FST videos. Solid lines, mean; shaded areas, s.e.m. AMF conditions: $H_0 = 45 \pm 2$ mT, $f = 164$ kHz. The blue area represents AMF exposure and the grey area indicates the absence of an AMF. *n*, number of test trials (which is the same as the number of subjects for the day 1–3 data, where one subject was tested per trial). **e**, Mice expressing hM3D(Gq) in the VTA neurons (hM3D(Gq)$^+$) and injected with CNO-loaded magnetoliposomes (CNO$^+$) exhibited enhanced swimming in response to the AMF stimulus (mean ± s.e.m., two-way ANOVA and Tukey's multiple comparisons test, $F_{3,122} = 5.387$, $^{**}0.001 \leq P < 0.01$, $^{****}P < 0.0001$). Pre, prestimulus epoch; dur, during AMF stimulation (or no AMF stimulation) epoch; post, poststimulus epoch. Each marker represents an FST trial and *n* represents the number of test trials. **f**, A repeated enhancement of swimming behaviour was observed in the hM3D(Gq)$^+$, CNO$^+$ group in response to AMF stimulation (two-way ANOVA and Tukey's multiple comparisons test, $F_{4,36} = 0.05789$, $P \geq 0.05$ (NS), $^{*}0.01 \leq P < 0.05$, $^{**}0.001 \leq P < 0.01$). NS, not significant; *n*, the number of subjects and test trials.

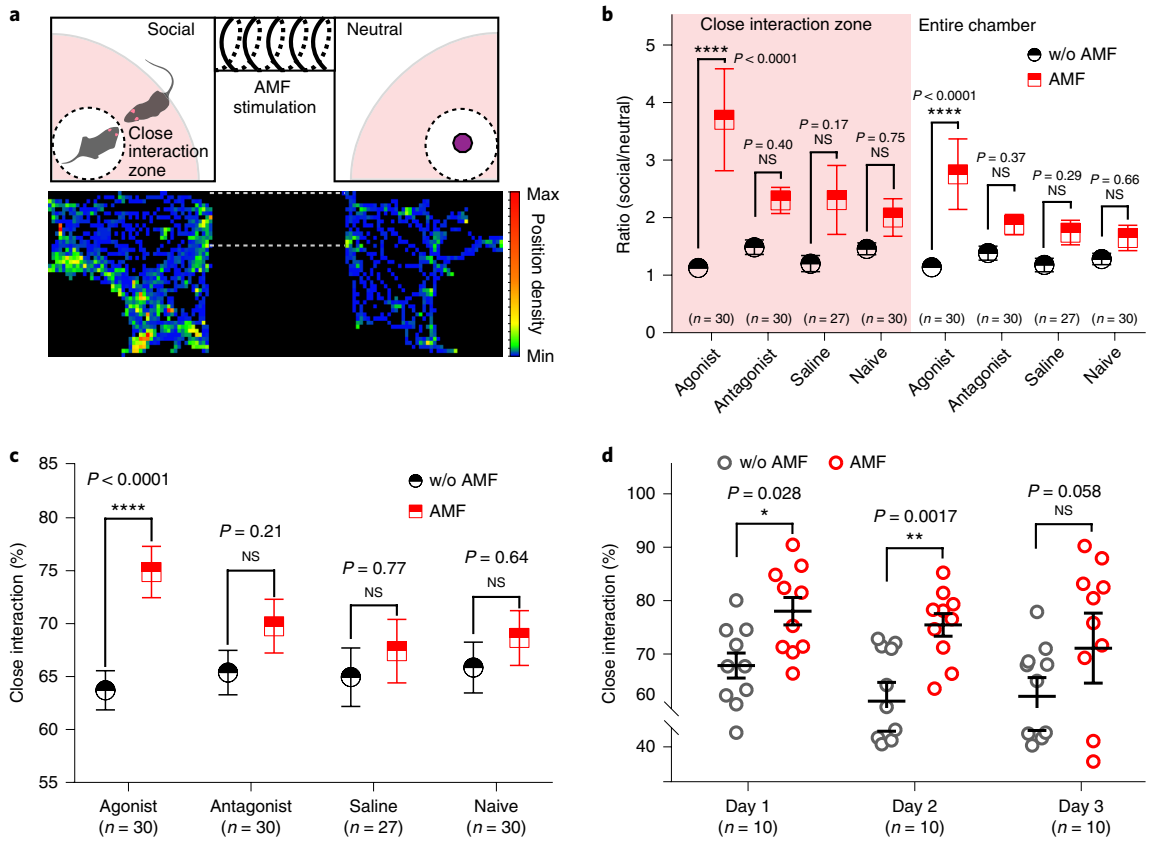

Fig. 4 | Remote chemomagnetic modulation mediated by endogenous receptors. a, Top: the experimental scheme for the mouse social preference test with an AMF coil that encompasses the middle chamber. The shaded radial area within the test chambers (90% of the chamber length and width) was defined as the close interaction zone. Bottom: a representative heat map that traces the position of a mouse in social subject and novel object chambers during the preference test. **b**, The ratio of time spent in the social interaction chamber to the object (neutral) chamber is compared for mice subjected to AMF. The group with agonist-loaded magnetoliposomes exhibited an enhanced social preference after exposure to AMF (mean ± s.e.m., two-way repeated measures ANOVA and Sidak's multiple comparisons test, close interaction $F_{3,113} = 3.053$, entire chamber $F_{3,113} = 3.547$, $^{****}P < 0.0001$). *n*, number of trials. **c**, The percentage of close interaction in the social chamber. The group injected with agonist-loaded magnetoliposomes spent more time in the close interaction zone (mean ± s.e.m., two-way repeated measures ANOVA and Sidak's multiple comparisons test, $F_{3,113} = 3.122$, $^{****}P < 0.0001$). *n*, number of trials. **d**, The group injected with agonist-loaded magnetoliposomes repeatedly showed an increased social preference after AMF exposure (mean ± s.e.m., two-way repeated measures ANOVA and Sidak's multiple comparisons test, $F_{2,27} = 0.5717$, $P \geq 0.05$ (NS), $^{*}0.01 \leq P < 0.05$, $^{**}0.001 \leq P < 0.01$). *n*, number of subjects and test trials (that is, one subject was tested per trial). w/o, without.

the DRD1 antagonist SCH-23390 or saline were loaded into the magnetoliposomes and then injected into the NAc of wild-type mice. Another group of wild-type mice that did not receive any material injection was set as naive group to investigate the potential influence of AMF alone on the social behaviour. A social preference assay compatible with chemomagnetic modulation was developed by constructing an AMF stimulation chamber connecting two test chambers that housed either a novel object or a novel mouse (Fig. 4a and Supplementary Fig. 14). Prior to the social preference assay, we confirmed that the mice did not exhibit a preference bias for either of the test chambers (Supplementary Fig. 15). During the social preference assay, the test mice were first confined to the stimulation chamber for 1 min of habituation and then exposed to 40 s of AMF. The mice were then released from the stimulation chamber to freely explore the two adjacent test chambers for 5 min. No significant differences in locomotor performance among the agonist, antagonist and saline groups were observed (Supplementary Fig. 16). Consistent with the activation of DRD1-expressing neurons in the NAc, only the mice injected with the DRD1 agonist-loaded magnetoliposomes displayed an increased social preference after the AMF stimulation (Fig. 4b,c and Supplementary Fig. 17). The ability of the magnetoliposomes to release multiple doses of their payloads has enabled a repeated control of sociability in the DRD1 agonist group, although the significance of the effect was reduced to a trend on the third day of exposure (Fig. 4d).

To evaluate the biocompatibility and stability of the magnetoliposomes in vivo, we examined the interface between these particles and the tissue. Four weeks after injection, magnetoliposomes were observable (Supplementary Fig. 18), but did not cause significant glial activation and macrophage accumulation (Supplementary Fig. 19). The minimal foreign body reaction by surrounding tissues may, in part, be attributed to the lipid-based chemistry of the magnetoliposomes[29] and the clinically assessed biochemical inertness of iron oxide nanoparticles[30]. No significant cytotoxicity was observed after AMF stimulation, neither in vitro (Supplementary Fig. 20) nor in vivo (Supplementary Fig. 21), consistent with the material inertness and negligible thermal effects of chemomagnetic stimulation.

We designed a chemomagnetic strategy that affords a spatially targeted and temporally precise molecular control of neural circuits by coupling a non-invasive magnetic field cue with magnetically responsive liposomal drug carriers. The magnetically gated small-molecule release facilitated a fast activation of both genetically engineered and endogenously expressed receptors within the

targeted neural populations during behavioural experiments. The chemomagnetic paradigm may, in future, be multiplexed to various ligand–receptor pairs to enable the remote modulation of multiple cell populations and to permit studies of drug interactions in behaving subjects[17].

Online content

Any methods, additional references, Nature Research reporting summaries, source data, statements of code and data availability and associated accession codes are available at https://doi.org/10.1038/s41565-019-0521-z.

Received: 31 August 2018; Accepted: 3 July 2019;
Published online: 19 August 2019

References

1. Harris-Warrick, R. M. & Marder, E. Modulation of neural networks for behavior. *Annu. Rev. Neurosci.* **14**, 39–57 (1991).
2. Smith, K. S., Bucci, D. J., Luikart, B. W. & Mahler, S. V. DREADDS: use and application in behavioral neuroscience. *Behav. Neurosci.* **130**, 137 (2016).
3. Sternson, S. M. & Roth, B. L. Chemogenetic tools to interrogate brain functions. *Annu. Rev. Neurosci.* **37**, 387–407 (2014).
4. Urban, D. J. & Roth, B. L. DREADDs (designer receptors exclusively activated by designer drugs): chemogenetic tools with therapeutic utility. *Annu. Rev. Pharmacol. Toxicol.* **55**, 399–417 (2015).
5. Shields, B. C. et al. Deconstructing behavioral neuropharmacology with cellular specificity. *Science* **356**, eaaj2161 (2017).
6. Misra, A., Ganesh, S., Shahiwala, A. & Shah, S. P. Drug delivery to the central nervous system: a review. *J. Pharm. Pharm. Sci.* **6**, 252–273 (2003).
7. Dagdeviren, C. et al. Miniaturized neural system for chronic, local intracerebral drug delivery. *Sci. Transl. Med.* **10**, eaan2742 (2018).
8. Chen, R., Romero, G., Christiansen, M. G., Mohr, A. & Anikeeva, P. Wireless magnetothermal deep brain stimulation. *Science* **347**, 1477–1480 (2015).
9. Schuerle, S., Dudani, J. S., Christiansen, M. G., Anikeeva, P. & Bhatia, S. N. Magnetically actuated protease sensors for in vivo tumor profiling. *Nano Lett.* **16**, 6303–6310 (2016).
10. Pankhurst, Q. A., Connolly, J., Jones, S. & Dobson, J. Applications of magnetic nanoparticles in biomedicine. *J. Phys. D.* **36**, R167–R181 (2003).
11. Huang, H., Delikanli, S., Zeng, H., Ferkey, D. M. & Pralle, A. Remote control of ion channels and neurons through magnetic-field heating of nanoparticles. *Nat. Nanotechnol.* **5**, 602 (2010).
12. Stanley, S. A. et al. Radio-wave heating of iron oxide nanoparticles can regulate plasma glucose in mice. *Science* **336**, 604–608 (2012).
13. Munshi, R. et al. Magnetothermal genetic deep brain stimulation of motor behaviors in awake, freely moving mice. *eLife* **6**, e27069 (2017).
14. Roth, B. L. DREADDs for neuroscientists. *Neuron* **89**, 683–694 (2016).
15. Yatvin, M. B., Weinstein, J. N., Dennis, W. H. & Blumenthal, R. Design of liposomes for enhanced local release of drugs by hyperthermia. *Science* **202**, 1290–1293 (1978).
16. Tai, L.-A. et al. Thermosensitive liposomes entrapping iron oxide nanoparticles for controllable drug release. *Nanotechnology* **20**, 135101 (2009).
17. Christiansen, M. G., Senko, A., Chen, R., Romero, G. & Anikeeva, P. Magnetically multiplexed heating of single domain nanoparticles. *Appl. Phys. Lett.* **104**, 213103 (2014).
18. Romero, G., Christiansen, M. G., Stocche Barbosa, L., Garcia, F. & Anikeeva, P. Localized excitation of neural activity via rapid magnetothermal drug release. *Adv. Funct. Mater.* **26**, 6471–6478 (2016).
19. Christiansen, M. G., Howe, C. M., Bono, D. C., Perreault, D. J. & Anikeeva, P. Practical methods for generating alternating magnetic fields for biomedical research. *Rev. Sci. Instrum.* **88**, 084301 (2017).
20. Chen, T.-W. et al. Ultrasensitive fluorescent proteins for imaging neuronal activity. *Nature* **499**, 295 (2013).
21. Gunaydin, L. A. et al. Natural neural projection dynamics underlying social behavior. *Cell* **157**, 1535–1551 (2014).
22. Lammel, S. et al. Input-specific control of reward and aversion in the ventral tegmental area. *Nature* **491**, 212 (2012).
23. Nestler, E. J. Is there a common molecular pathway for addiction? *Nat. Neurosci.* **8**, 1445–1149 (2005).
24. Tye, K. M. et al. Dopamine neurons modulate neural encoding and expression of depression-related behaviour. *Nature* **493**, 537–541 (2013).
25. Morales, M. & Margolis, E. B. Ventral tegmental area: cellular heterogeneity, connectivity and behaviour. *Nat. Rev. Neurosci.* **18**, 73–85 (2017).
26. Sagar, S., Sharp, F. & Curran, T. Expression of c-fos protein in brain: metabolic mapping at the cellular level. *Science* **240**, 1328–1331 (1988).
27. Mul, J. D., Zheng, J. & Goodyear, L. J. Validity assessment of 5 day repeated forced-swim stress to model human depression in young-adult C57BL/6J and BALB/cJ mice. *eNeuro* **3**, 0201–0216 (2016).
28. Rahman, S. & McBride, W. J. D1–D2 dopamine receptor interaction within the nucleus accumbens mediates long-loop negative feedback to the ventral tegmental area (VTA). *J. Neurochem.* **77**, 1248–1255 (2001).
29. Naahidi, S. et al. Biocompatibility of engineered nanoparticles for drug delivery. *J. Control Release* **166**, 182–194 (2013).
30. Laurent, S. et al. Magnetic iron oxide nanoparticles: synthesis, stabilization, vectorization, physicochemical characterizations, and biological applications. *Chem. Rev.* **108**, 2064–2110 (2008).

Acknowledgements

We thank B. Roth, D. Kim and F. Zhang for the generous gifts of the plasmids and cell lines, Z. He, Y. Lin, the Viral Core of Boston Children's Hospital and the University of Pennsylvania Vector Core for packaging of the AAVs and for the support and advice on virus packaging, A. Galal for the scripts used in the analysis of behaviours and S. Lall and A. Jasanoff for their thoughtful comments on our manuscript. This work was funded in part by DARPA ElectRx Program under D. Weber (HR0011-15-C-0155), the Bose Research Grant and the National Institutes of Health BRAIN Initiative (1R01MH111872). This work made use of the Massachusetts Institute of Technology (MIT) MRSEC Shared Experimental Facilities under award no. DMR-14-19807. S.R. and R.C. are supported by a grant from the Simons Foundation to the Simons Center for the Social Brain at MIT. Methods of analysis and additional data are included in the Supplementary Information.

Author contributions

S.R., R.C. and P.A. designed all the experiments and performed all the analyses. M.G.C. and A.W.S. designed and constructed the magnetic field coils. S.R., R.D. and J.M. developed the magnetoliposome preparation methods. P.-H.C. constructed the DNA plasmids. S.R. and J.X. packaged the viral vectors. S.R., A.A.L., C.H.S. and Y.Z. conducted behavioural experiments and analyses. S.R., A.A.L. and C.H.S. conducted the immunohistochemistry analyses. G.V. and A.A.L. wrote the scripts for the automatic classifier used for the FST assays. C.H.S. wrote the scripts for calcium imaging visualization and social behaviour analyses. G.F. advised on social preference assays and facilitated the analysis of behavioural data. S.R. and S.P. conducted the statistical analysis. All the co-authors contributed to the writing of the manuscript.

Competing interests

The authors declare no competing interests.

Additional information

Supplementary information is available for this paper at https://doi.org/10.1038/s41565-019-0521-z.

Reprints and permissions information is available at www.nature.com/reprints.

Correspondence and requests for materials should be addressed to P.A.

Peer review information: *Nature Nanotechnology* thanks Joao Carvalho-de-Souza, Patricia Janak and Shan Wang for their contribution to the peer review of this work

Publisher's note: Springer Nature remains neutral with regard to jurisdictional claims in published maps and institutional affiliations.

Methods

Molecular cloning and virus packing. For the construction of pLenti-CamKIIα-hM3D(Gq)-p2A-mCherry, we first obtained the hM3D(Gq) fragment from pAAV-CaMKIIα-hM3D(Gq)-mCherry (a gift from B. Roth, Addgene plasmid no. 50476) by PCR with the primers 5′-GGGCAGCGGGGGATCCGCCACCA TGACCTTGCACAATAAC-3′ and 5′-GGAGCCGGGCGCGCCTTTCAAGG CCTGCTCGGGTG-3′. The linearized vector was obtained from pLenti-CamKIIα-TRPV1-p2A-mCherry (developed in house)[8] by PCR with primers 5′-GGATCCCCCGCTGCCCC-3′ and 5′-GGCGCGCCCGGCTCC-3′. The hM3D(Gq) was cloned into the p2A construct, replacing TRPV1. pAAV-hSyn-hM3D(Gq)-mCherry was a gift from B. Roth (Addgene plasmid no. 50474 and Addgene viral preparation no. 50474-AAV5). pGP-CMV-GCaMP6s was a gift from D. Kim (Addgene plasmid no. 40753). AAV5-hSyn-mCherry and AAV9-hSyn-hM3D(Gq)-mCherry were prepared by Boston Children's Hospital viral core. pAAV-hSyn-GCaMP6s-WPRE-SV40 was a gift from The Genetically Encoded Neuronal Indicator and Effector Project (GENIE) and D. Kim (Addgene viral preparation no. 100843-AAV9). Prior to use, all the viral vectors were diluted to a titre of 10^{12} transducing units per millilitre.

Magnetoliposome preparation. Amine-terminated iron oxide MNPs (25 nm) (Ocean NanoTech, SHA 25)[9], DPPC (Avanti Polar Lipids, 850355), DSPC (Avanti Polar Lipids, 850365) and cholesterol (Sigma-Aldrich, C8667) were used for the magnetoliposome preparation. The lipid mixture was first dissolved in dichloromethane and the aqueous phase (MNPs with payloads) was added into the lipid mixture. After homogenization (>6,000 r.p.m.), the second water-phase solution was added followed by quick vortex mixing. Then, evaporation was rapidly applied and kept for more than 30 min. For further purification, a magnetic separator was used (Ocean NanoTech, SuperMag-01). The payload concentration and second water-phase solution are summarized in Supplementary Table 2.

Cell culture. A hippocampal culture was isolated from neonatal rat pups (P1) and dissociated with Papain (Worthington Biochemical). After physical trituration, dissociated neural cells were plated on 5 mm diameter glass slides in 24 well plates. The glass slides were cleaned by hydrochloric acid treatment, washed with sterile 70% ethanol in water and then sterile water, and then coated with Matrigel (Corning). The cells were maintained in Neurobasal media (Invitrogen). Glial inhibition with 5-fluoro-2′-deoxyuridine (FUDR, F0503 Sigma) was conducted 3 days after seeding the cells, and then the culture was transfected with 1 µl of an AAV9 cocktail of hSyn::GCaMP6s and hSyn::hM3D(Gq)-mCherry or hSyn::mCherry. After a 5 day incubation period, calcium imaging experiments were performed on the transfected cultures.

The HEK 293FT cell line was a gift from F. Zhang (MIT) and maintained in DMEM (with GlutaMax) + 10% fetal bovine serum. To facilitate the imaging with AMF stimulation, the HEK cells were plated onto the Matrigel-coated 5 mm diameter glass slides in 24 well plates. Lipofectamine 2000 was used for all the transfections. We used 1 µl of Lipofectamine and 500 ng of DNA per 500 µl of media within each well.

In vivo studies. All the experimental procedures were approved by the MIT Committee on Animal Care.

Adult male C57BL/6 mice (Jackson Laboratory) aged 8 weeks were used for the c-fos quantification, behavioural assays and fibre photometry experiments. Mice were group housed with the exception of those implanted with optical fibres, and were on a reverse 12 h light/dark cycle with food and water ad libitum.

Virus and magnetoliposome injection, and optical fibre implantation. Mice were anaesthetized with isoflurane (0.5–2.5% in O_2) using a rodent anaesthesia machine (VetEquip) and positioned within a stereotaxic frame (David Kopf Instruments). During the surgical procedures, ophthalmic ointment was applied to the eyes to prevent drying. All the injections were conducted with a micro-injection apparatus (10 µl Nanofil Syringe, bevelled 34-gauge needles facing the dorsolmedial side, UMP-3 syringe pump, and its controller Micro4 (World Precision Instruments)) at an infusion rate of 100 nl min^{-1}. During the injections, the syringe was elevated by 100 µm from the initial coordinates. After the injections, the syringe needles remained inside the brain for another 10 min prior to a slow withdrawal.

For the c-fos quantification and FST assays, 300 nl of AAV5-hSyn:: hM3D(Gq)-mCherry or hSyn::mCherry with a titre of 10^{12} U ml^{-1} were injected bilaterally into the VTA, with the coordinates relative to bregma according to the *Allen Mouse Brain Atlas*: −3.08 mm anteroposterior (AP), ±0.4 mm mediolateral (ML), −5 mm dorsoventral (DV). Magnetoliposomes (1 µl, ~15 µg ml^{-1}) were also bilaterally injected into the same coordinates. For the fibre photometry experiments, 600 nl of an AAV9 cocktail of hSyn:: hM3D(Gq)-mCherry or hSyn::mCherry and hSyn::GCaMP6s was injected unilaterally into the VTA, as well as 1 µl of magnetoliposomes. The optical fibres were implanted above the virally transduced volume with the coordinates −3.08 mm AP, +0.4 mm or −0.4 mm ML, −4.8 mm DV. For social preference experiments, magnetoliposomes were bilaterally injected into the NAc (coordinates +1.25 mm AP, ±0.75 mm ML, −4.5 mm DV).

After all the injection surgeries, the skin over the mouse skull was closed with sutures. During the fibre implantation surgeries, the fibres were fixed onto the skull with multiple layers of adhesive (C&B Metabond, Parkell) and dental cement (Lang Dental, Jet Set-4). All the mice were given a subcutaneous injection of sustained-release buprenorphine (Bup-SR) (1 mg kg^{-1}) during surgery and warm lactated Ringers solution during recovery.

Immunohistochemistry analysis. For the c-fos quantification, mice were transfected with AAV5-hSyn::hM3D(Gq)-mCherry or hSyn::mCherry in the VTA, which was followed by a 5–6 week incubation period followed by the magnetoliposomes injection into the same location. After a recovery period of 3 days, mice were anaesthetized via an intraperitoneal injection of a ketamine (100 mg kg^{-1}) and xylazine (10 mg kg^{-1}) mixture and transferred to the magnetic coil for stimulation. The mice were subjected to a sequence of five AMF exposures ($f = 164$ kHz and $H_0 = 45 \pm 2$ mT) with 40 s ON, followed by 40 s OFF, and then transferred back to their home cages for 90 min to allow for c-fos expression. The mice were then euthanized by a lethal intraperitoneal injection of a sodium pentobarbital (Fatal-plus, 390 mg ml^{-1}, dose 0.5 mg g^{-1}) followed by transcardial perfusion as described below.

For all the immunohistochemistry studies, the mice were transcardially perfused with 4% paraformaldehyde in PBS, and their brains were extracted and kept in 4% paraformaldehyde solution overnight at 4 °C. The fixed brain samples were then sectioned into 40 µm thick coronal slices using a vibrating blade microtome (Leica VT1000S). The slices were permeabilized and blocked for 1 h in the dark at room temperature in a 0.3% v/v Triton X-100 and 3% v/v blocking serum solution in PBS in an orbital shaker. After three washes with PBS, the brain slices were incubated in primary antibody solution (with 3% blocking serum) overnight at 4 °C. After another three washes with PBS, the brain slices were transferred into a secondary antibody solution and incubated in the dark for 3 h at room temperature. After a further three washes with PBS, the brain slices were transferred onto glass slides and mounted with mounting medium (VECTASHIELD that contained DAPI nuclear stain). The primary antibodies, blocking serum and secondary antibodies for the c-fos quantification and biocompatibility analyses are summarized in Table 1.

Fibre photometry. In the fibre photometry set-up, the 473 nm diode laser (OEM Laser Systems, 50 mW peak power) was controlled by a function generator (Agilent, 33500B Series, 400 Hz, square wave) and coupled to a 3 m long modified ferrule rotary joint patch cable with a 400 µm core (Thorlabs, RJPFL4) using a 20×0.45 NA microscope objective (Olympus) integrated with a fibre launch stage (Thorlabs, MBT610D). Optical fibres (Thorlabs, FP400URT, 400 µm, 0.48 NA) outfitted with ceramic ferrules (Thorlabs, CF440-10) were implanted into mice and could be connected to the photometry patchcord linked to the fibre launch using ceramic split mating sleeves (Thorlabs, ADAF1-5). The laser intensity out of the coupled fibre tip was set between 100 and 200 µW. The GCaMP6s fluorescence was collected by the same implanted optical fibre and transmitted through the objective and the dichroic mirror (Thorlabs, CM1-DCH). The collected fluorescence was then longpass filtered to eliminate any remaining laser background (Semrock, BLP01-473R-25) onto a femtowatt silicon photoreceiver (Newport, NewFocus 2151, a.c. high mode). The photoreceiver was directly connected to a lock-in amplifier (Stanford Research Systems, SR830 DSP, 8 ms time constant) and recorded by custom software written in LabView with an acquisition frequency of 8.5 Hz. All the fibre photometry experiments were performed during the dark phase of the light/dark cycle in the dark, and the fibre patch cord was suspended above the magnetic coil to allow the mice to move freely during stimulation. The mice were acclimated to the photometry room for ≥1 h and to the magnetic coil for ≥15 min prior to recording.

Behavioural assays. In all the behavioural experiments, adult male mice (C57BL/6, aged 8 weeks at the start of experimental procedures) were used during the dark phase of the light/dark cycle, and were acclimated to the behaviour room for ≥1 h

Table 1 | Antibodies and blocking serum

Primary antibody	Blocking serum	Secondary antibody
Rabbit anti-cfos[34] (1:500, Cell Signaling Technology, 2250s)	Normal donkey serum	Donkey anti-rabbit, Alexa Fluor 488 (1:1,000, Invitrogen, A-21206)
Goat anti-GFAP[35] (1:1000, Abcam, ab53554)	Normal donkey serum	Donkey anti-goat, Alexa Fluor 488 (1:1,000, Invitrogen, A-11055)
Goat anti-Iba1[35] (1:500, Abcam, ab107159)	Normal donkey serum	Donkey anti-goat, Alexa Fluor 488 (1:1,000, Invitrogen, A-11055)
Cleaved Caspase-3 (1:500, Cell Signaling Technology, 9661s)	Normal donkey serum	Donkey anti-rabbit, Alexa Fluor 488 (1:1,000, Invitrogen, A-21206)

prior to testing. In the social preference assays, adult male mice (C57BL/6, aged 5–6 weeks) were used as strangers.

For the FST assay, a transparent plastic cylinder fitting into the magnetic field coil was used as a swimming tank. On day 0, all the mice were subjected to 6 min of pretest swimming, and on the subsequent three test days, each mouse experienced a 6 min swimming session each day. The first 180 s of the 6 min FST was set as the prestimulus epoch, then 40 s of AMF stimulation (or without AMF stimulation) was applied between 180 and 220 s, defined as the during-stimulus epoch, with the remaining 220–300 s defined as a poststimulus epoch. The water temperature was maintained at 28 °C. Mobility percentage was calculated as a ratio of the time that each mouse spent moving to the total time of each epoch.

For the social preference assay, two square chambers with dimensions 20 cm × 20 cm × 15 cm (length × width × height) were connected with a cylindrical tunnel surrounded by the magnetic field coil. Two gates were set at the entrances into the tunnel to confine the test mice to the stimulation chamber. During each trial, a test mouse was confined inside the magnetic coil stimulation chamber for 1 min as habituation, and then exposed to 40 s of AMF stimulation (or without AMF stimulation). The gates were then lifted and the mouse allowed to freely explore the two test chambers for 5 min. On day 0, all the test mice were subjected to this experimental method in the absence of novel objects and social strangers in the chambers. During the following 3 days, each mouse was tested without AMF stimulation and with AMF stimulation on each day. The preference (social/neutral) was calculated as the ratio of the time spent in the social chamber (or in the social close interaction zone) to the time spent in the neutral chamber (or the neutral chamber close interaction zone) for each test mouse. In each trial, the locations of the new object and the stranger were counterbalanced, and a new stranger and object were presented. The central luminous power of each chamber was maintained at 180–190 lux (Grainger).

Analysis scripts. In the FST experiments, mouse movements were tracked using the Behavioral Monitoring Tool[31]. The mobility energy was calculated from the difference in the pixel intensity of successive grayscale frames in the FST videos. Specifically, for each two successive frames the difference in greyscale intensity of each pixel was computed. If the absolute value of this difference was larger than a lower threshold, then the pixel difference was accumulated towards the total frame difference. This yielded a one-dimensional array of total greyscale intensity changes. To obtain the final mobility energy, we performed the following three operations: first, the intensity changes were normalized to account for varying frame sizes; second, a low-pass filter was applied to the array to remove noise due to abrupt changes in light and, finally, a moving average filter was applied to obtain a smooth mobility energy curve. In the social preference experiments, the mice movements were tracked by ToxTrac[32,33] and the analysis was conducted using custom scripts written in Mathematica (Wolfram).

Reporting summary. Further information on research design is available in the Nature Research Reporting Summary linked to this article.

Data availability

The data that support the findings of this study are presented within the manuscript and are available from the corresponding author upon request.

Code availability

All the scripts are available from the corresponding author upon request.

References

31. Galal, A. *Behavioral Monitoring Tool* http://ratmonitoring.sourceforge.net (2001).
32. Rodriguez, A. et al. ToxTrac: a fast and robust software for tracking organisms. *Methods Ecol. Evol.* **9**, 460–464 (2018).
33. Rodriguez, A., Zhang, H., Klaminder, J., Brodin, T. & Andersson, M. ToxId: an efficient algorithm to solve occlusions when tracking multiple animals. *Sci. Rep.* **7**, 14774 (2017).
34. Zhu, X.-N. et al. Ephrin-B3 coordinates timed axon targeting and amygdala spinogenesis for innate fear behaviour. *Nat. Commun.* **7**, 11096 (2016).
35. Park, S. et al. One-step optogenetics with multifunctional flexible polymer fibers. *Nat. Neurosci.* **20**, 612–619 (2017).

nature research

Corresponding author(s): DBPR NNANO-18081878A, Polina Anikeeva

Last updated by author(s): Jul 1, 2019

Reporting Summary

Nature Research wishes to improve the reproducibility of the work that we publish. This form provides structure for consistency and transparency in reporting. For further information on Nature Research policies, see Authors & Referees and the Editorial Policy Checklist.

Statistics

For all statistical analyses, confirm that the following items are present in the figure legend, table legend, main text, or Methods section.

n/a	Confirmed
☐	☒ The exact sample size (*n*) for each experimental group/condition, given as a discrete number and unit of measurement
☐	☒ A statement on whether measurements were taken from distinct samples or whether the same sample was measured repeatedly
☐	☒ The statistical test(s) used AND whether they are one- or two-sided *Only common tests should be described solely by name; describe more complex techniques in the Methods section.*
☐	☒ A description of all covariates tested
☐	☒ A description of any assumptions or corrections, such as tests of normality and adjustment for multiple comparisons
☐	☒ A full description of the statistical parameters including central tendency (e.g. means) or other basic estimates (e.g. regression coefficient) AND variation (e.g. standard deviation) or associated estimates of uncertainty (e.g. confidence intervals)
☐	☒ For null hypothesis testing, the test statistic (e.g. *F*, *t*, *r*) with confidence intervals, effect sizes, degrees of freedom and *P* value noted *Give P values as exact values whenever suitable.*
☒	☐ For Bayesian analysis, information on the choice of priors and Markov chain Monte Carlo settings
☒	☐ For hierarchical and complex designs, identification of the appropriate level for tests and full reporting of outcomes
☒	☐ Estimates of effect sizes (e.g. Cohen's *d*, Pearson's *r*), indicating how they were calculated

Our web collection on statistics for biologists contains articles on many of the points above.

Software and code

Policy information about availability of computer code

Data collection	In forced swimming test assays mouse movements were tracked using an open source Behavioral Monitoring Tool, which can be found at http://ratmonitoring.sourceforge.net. In the social preference assays, the mice movements were tracked by an open source ToxTrac, which can be found at https://sourceforge.net/p/toxtrac/wiki/Home/.
Data analysis	For the forced swimming test and social preference assays, the analyses were conducted using custom scripts written in Mathematica (11.3 Wolfram) software. All codes are available upon request.

For manuscripts utilizing custom algorithms or software that are central to the research but not yet described in published literature, software must be made available to editors/reviewers. We strongly encourage code deposition in a community repository (e.g. GitHub). See the Nature Research guidelines for submitting code & software for further information.

Data

Policy information about availability of data

All manuscripts must include a data availability statement. This statement should provide the following information, where applicable:

- Accession codes, unique identifiers, or web links for publicly available datasets
- A list of figures that have associated raw data
- A description of any restrictions on data availability

All datasets generated during this study and the analysis scripts are available from the corresponding author upon request.

Field-specific reporting

Please select the one below that is the best fit for your research. If you are not sure, read the appropriate sections before making your selection.

☒ Life sciences ☐ Behavioural & social sciences ☐ Ecological, evolutionary & environmental sciences

For a reference copy of the document with all sections, see nature.com/documents/nr-reporting-summary-flat.pdf

Life sciences study design

All studies must disclose on these points even when the disclosure is negative.

Sample size	For in vitro microscopy imaging experiments, 3-5 videos were imaged to inspect >100 cells per experimental condition; for the c-fos immunohistological experiments, 3-5 mice were injected and their tissue imaged per experimental condition; for the fiber photometry experiments, 3 mice were used per experimental group; for the forced swimming test assays, total of 40 mice were injected and tested in the behavior experiments; for the social preference assays, total of 39 mice were injected and tested in the behavior experiments. Sample sizes for behavioral experiments were informed by the number of subjects reported for similar studies, based on the minimal number of mice required to detect significance with an alpha rate set at .05 in a standard power experiment.
Data exclusions	Imaged neurons were excluded based on the expression level (i.e. no detectable expression) of the designed receptors (hM3Dq-mcherry or mcherry). Trials in forced swimming tests were excluded based on the identification of adaption in tests. The mouse mobility datasets were automatically selected without bias via the scripts to identify adaptation behavior in trials. The scripts fit the mobility datasets with a linear combination of Gaussian distributions, and the subjects classified as belonging to a mobility distribution centered around 0% prior to exposure to magnetic field were considered to have adapted and were used in analyses. The algorithm and adaptation identification are described in the manuscript. No mice nor trials were excluded from the social preference assays.
Replication	Each in vitro experiment was repeated in 3-5 times per experimental condition. Each in vivo experiment was repeated in 3-10 subjects per experiment. All results in the paper are drawn from the analysis of multiple animals, all numbers are indicated in text and figure captions. In the forced swimming tests and social preference assays, the same cohort of mice were subjected to the behavioral paradigms for 3 consecutive days.
Randomization	Cultured cells were randomly and automatically chosen for each experimental paradigm, Animals were assigned randomly to each experimental group.
Blinding	The investigators were not blinded during in vitro stimulation nor behavior data collection. A separate naive group of blinded investigators conducted data analysis.

Reporting for specific materials, systems and methods

We require information from authors about some types of materials, experimental systems and methods used in many studies. Here, indicate whether each material, system or method listed is relevant to your study. If you are not sure if a list item applies to your research, read the appropriate section before selecting a response.

Materials & experimental systems

n/a	Involved in the study
☐	☒ Antibodies
☐	☒ Eukaryotic cell lines
☒	☐ Palaeontology
☐	☒ Animals and other organisms
☒	☐ Human research participants
☒	☐ Clinical data

Methods

n/a	Involved in the study
☒	☐ ChIP-seq
☒	☐ Flow cytometry
☒	☐ MRI-based neuroimaging

Antibodies

Antibodies used	Primary antibodies: Rabbit anti-cfos (Cell Signaling technology, 2250s), Goat anti-GFAP (Abcam, ab53554), Goat anti-Iba1 (Abcam, ab107159), Cleaved Caspase-3 (Cell Signaling technology, 9661s) Secondary antibodies: Donkey anti-Rabbit, Alexa Fluor 488 (Invitrogen, A-21206), Donkey anti-Goat, Alexa Fluor 488 (Invitrogen, A-11055)
Validation	The antibodies were validated in literature and in our laboratory for immunohistological staining on mouse brain slices (adult, C57BL/6).

Eukaryotic cell lines

Policy information about cell lines

Cell line source(s)	The HEK 293FT cell line was a gift by Feng Zhang (MIT)
Authentication	Microscopic inspection
Mycoplasma contamination	The cell line is negative for mycoplasma contamination
Commonly misidentified lines (See ICLAC register)	N/A

Animals and other organisms

Policy information about studies involving animals; ARRIVE guidelines recommended for reporting animal research

Laboratory animals	Adult male C57BL/6 mice (Jackson Laboratory) aged 8 weeks were used in the experiments.
Wild animals	N/A
Field-collected samples	N/A
Ethics oversight	All experimental procedures were approved by the MIT Committee on Animal Care

Note that full information on the approval of the study protocol must also be provided in the manuscript.